Journal of Directed Energy, **3**, Spring 2009, 134–148

HAL: Humidity and Aerosol LIDAR for Profiling Atmospheric Water Vapor and Aerosols

J. P. Sherman*

Department of Physics and Astronomy, Appalachian State University, 531 Rivers Street, CAP Building Room 231, Boone, North Carolina 28608

and

P. D. Dao†

Air Force Research Laboratory/RVBYB, 29 Randolph Road, Hanscom Air Force Base, Massachusetts 01731

The design and initial field testing of a prototype water vapor differential absorption LIDAR (DIAL) developed at the Air Force Research Laboratory are discussed in this paper. The operational version of a steerable LIDAR, named HAL (humidity and aerosol LIDAR), will profile line-of-sight aerosols and water vapor with high spatial and temporal resolution along downward-pointing, long-slant paths during clear-sky and moderately turbid conditions as a support tool for tactical high-energy laser experiments. A high pulse-energy alexandrite transmitter produces more than 1 W of narrow-line average power at the 729.23-nm H_2O vapor line, permitting high resolution using a modest receiver aperture. Stable transmitter operation for continuous periods exceeding 30 h has been demonstrated. The prototype LIDAR was pointed upward for direct and indirect comparisons of LIDAR-derived absolute humidity profiles with colocated and regionally launched radiosondes and with a colocated microwave radiometer. Qualitative (and often quantitative) agreement was observed for upward-pointing water vapor retrievals up to 4.5-km (3.5 km) altitudes during nighttime (daytime) hours, in addition to qualitative aerosol layer/cloud profiles up to 14 km. The H_2O vapor range will be expanded by a modified receiver currently being developed. Potential applications include characterizing the effects of water vapor and aerosols on high-energy electromagnetic wave propagation and cloud prediction.

KEYWORDS: Aerosols, Beam propagation, DIAL, Thermal blooming, Water vapor

Nomenclature

$n_{H_2O}(z)$	water vapor molecular density (g/cm^3) at altitude z (m)
$P_{ON}(z)/P_{OFF}(z)$	detected backscatter from altitude z (m) at the on-resonance/off-resonance laser operating wavelength [Eq. (1)]

Received November 12, 2008; revision received April 13, 2009.
*Corresponding author; e-mail: shermanjp@appstate.edu.
†E-mail: afrl.rvb.pa@hanscom.af.mil.

$\Delta n_e(z)$	differential extinction correction term to the water vapor density [Eq. (1)]
$\Delta n_\beta(z)$	differential backscatter correction term to the water vapor density [Eq. (1)]
$\lambda_{ON}/\lambda_{OFF}$	on-resonance/off-resonance laser operating wavelength
σ_{ON}/σ_{OFF}	water vapor absorption cross section (cm^2) at the on-resonance/off-resonance laser operating wavelength [Eq. (1)]

1. Introduction

Water vapor is an atmospheric constituent with high temporal and spatial variability. Its variability affects a number of natural and meteorological phenomena such as cloud formation, propagation of electromagnetic radiation, and the balance of heat flux at local and global scales, in addition to modifying the radiative properties of hygroscopic aerosols. To investigate these phenomena, accurate measurements of atmospheric water vapor data with high spatial and temporal resolution are needed. In the engineering research community, there is also interest in characterizing and predicting the propagation of high-energy laser (HEL) beams through long-slant ranges.[15] The beam irradiance and phase profile can be altered significantly by scattering and absorption due to molecules and aerosols and by turbulent small-scale humidity fluctuations present along the beam path. The effect of most aerosol types (except for soot and organic aerosols produced by biomass burning) on a near-infrared (near-IR) laser beam is primarily to attenuate the beam by scattering incident energy. Molecular water vapor has a wealth of absorption bands throughout the near-IR and IR, and its absorption of HEL beam energy has the effect of heating the local atmosphere along the beam path, resulting in reduced local refractive index and increased beam divergence (thermal blooming effect).[2] Turbulent small-scale humidity fluctuations can under certain conditions contribute significantly to optical refractive index fluctuations in the lower troposphere,[7] resulting in increased scintillation or beam intensity fluctuations over an extended path. These effects all lead to reduced beam irradiance delivered to a target and must be accounted for in performance models for any tropospheric-operating HEL system whose wavelength does not lie in a water vapor transmission window. One example is the chemical oxygen–iodine laser (COIL), operating at 1.31525 μm, which experiences absorption in the lower troposphere due to pressure broadening of several nearby H_2O absorption lines. Because thermal blooming effects depend superlinearly on local beam irradiance, the water vapor profiles must possess high spatial and temporal resolution.

Differential absorption LIDAR (DIAL) is a powerful active remote sensing technique for retrieving range-resolved H_2O vapor density (or mixing ratio) and aerosol Mie backscatter profiles.[4,13] Water vapor DIAL utilizes the laser light backscattered from atmospheric aerosols and molecules at two closely spaced laser wavelengths: one wavelength λ_{ON} residing at the peak of a narrow H_2O vapor absorption line and a second wavelength λ_{OFF} that lies just outside the absorption line. In such cases, the wavelength difference $\lambda_{ON} - \lambda_{OFF}$ is very small and the difference between the two backscattered signals collected by a receiving telescope is solely due to differential absorption by water vapor along the beam path. High-resolution profiles of water vapor density are derived by measuring the ratio of backscattered light at the two wavelengths as a function of range from the LIDAR. With suitable data processing, the off-resonance LIDAR backscatter can also be utilized to obtain quantitative line-of-sight aerosol profiles.[9] In comparison to the more mature

technique of Raman LIDAR, DIAL requires a lower telescope aperture–laser power product and offers the possibility of daytime operation. Unlike Raman and Rayleigh–Mie LIDARs, DIAL requires no calibration constants or assumptions. As such, it is the only remote sensing technique to date that provides absolutely calibrated water vapor profiles without the need to rely on other instruments.[16] In situ measurements by balloon-borne radiosondes, used in this study for benchmark comparison, provide the highest spatial resolution, but infrequent launches would not provide the desired temporal resolution. Passive radiometric measurements at microwave wavelengths can produce profiles, but detailed water-vapor structure is not expected from the inversion technique.

The Battlespace Environment Division of the Space Vehicles Directorate was awarded one of the first High Energy Laser Joint Technology Office (HEL–JTO) grants to study atmospheric impacts to tactical HEL systems (JTO-02-0602-19). The prototype DIAL sensor discussed in this paper, initiated by Dao and Dentamaro,[5] represents a scalable proof-of-concept version of a steerable humidity and aerosol LIDAR (HAL) that will provide support for high-energy tactical laser experiments via high-resolution, line-of-sight H_2O vapor and qualitative aerosol profiles. The operational version of HAL will be a downward-looking diagnostic tool to determine H_2O vapor profiles along a slant path, with the end point situated on the ground. We define high resolution (for the purpose of this application) as a few minutes temporal and 100–200 m spatial over the path length for H_2O vapor profiles and tens of meters for qualitative aerosol backscatter retrievals. The profiles will provide real-time diagnosis of the presence of aerosol layers or water vapor levels sufficiently high so as to preclude effective laser energy transmission to the target. The sensor will operate under clear-sky and partly cloudy conditions, where if necessary the laser can be pointed around the clouds to reach the target. The design range of the operational sensor is close to 10 km when pointed along a downward-slant path. The receiver aperture of the operational system is scalable by a factor of two from the prototype system, so the latter should possess a range of close to 5 km. Range is limited under clear-sky conditions by the amount of Rayleigh backscattering, which is proportional to the quotient of molecular density and the square of range at the far end of the range.[9] Owing to higher far-end molecular densities when the LIDAR is pointing downward (along with lower sky background radiance levels), the listed requirement corresponds to a minimum of ca. 4 km for the vertical-pointing prototype. Another factor benefiting the downward-pointing operational LIDAR is much higher water vapor absorption at the far end of the range. For tactical applications, the retrieved water vapor profiles should possess accuracies of ~ 2 g/m^3 along the path, which corresponds to roughly 20%–30% of typical surface-level values. The off-resonance return also provides an indicator of the aerosol's presence along a line of sight. For low to moderate attenuation, a LIDAR ratio ranging from 25 to 80 sr as reported by Ackermann[1] can actually be used to coarsely estimate extinction. Note that in Ackermann's paper, the ratios were calculated at the three Nd:YAG wavelengths that bracket the alexandrite wavelength. Although the prototype LIDAR is a demonstration of the line-of-sight diagnosis, there is no attempt to achieve the actual capability of the operational LIDAR. In some areas, the design criteria of the demonstration LIDAR are so different from the operational unit that the range of operation is not the same. For example, the bistatic receiver of the demonstration LIDAR is not expected to provide quantitative backscatter information in the near field because of incomplete beam–receiver overlap.

Another potential future application of the operational version of HAL is to predict the onset of clouds. Free-space optical communication and missile defense applications

require a clear path between transmitter and receiver/target. In addition to attenuating the laser signal, cloud droplets scramble the transmitted data bits via temporal broadening of the laser pulses. Observations from ORCLE and ABL_CI field experiments conducted at Hanscom Air Force Base[10] have revealed the presence of a moist layer both before clouds are manifest in that layer and during the dissipative stages of the cloud layer. Trends in time-resolved water vapor and aerosol backscatter profiles obtained during the formation and dissipation of cloud layers should result in a better understanding of how such clouds form and dissipate. This knowledge could then be utilized to more accurately forecast visibility along the field of view,[11] which in turn could be used to determine whether to use optical or microwave transmitter radiation sources.

2. Prototype HAL System

2.1. Transmitter

Requirements of a DIAL transmitter include a stable, narrow-bandwidth laser capable of switching rapidly between two wavelengths whose locations are precisely known, relative to the peak of an absorption line of known cross section. Narrow bandwidth is defined here such that the laser linewidth is much narrower (in practice, by a factor of at least 10) than the absorption linewidth of the probed species,[14] so that its effect on the spectral properties of the retrieved backscatter can, to first order, be neglected. Near-IR water vapor linewidths typically range from approximately 6 GHz full-width-at-half-maximum (FWHM) at the surface to slightly less than 2 GHz near 10 km, necessitating (according to our criteria) a transmitter linewidth of less than 200 MHz. Wavelength switching on the order of milliseconds is necessary so that both the on- and off-resonance beams sample the same air mass. Both LIDAR operating wavelengths λ_{ON} and λ_{OFF} must be precisely known in order to deduce gas number concentration (via the differential absorption cross section) profiles from the retrieved backscatter profiles. Water vapor possesses three near-IR absorption bands (720–730, 820–830, and 900–950 nm). The shortest wavelength band was chosen for the initial studies to (1) maximize Rayleigh backscatter from air molecules (necessary for operation during periods of low aerosol loading), (2) maximize the H_2O vapor measurement range during humid months (due to lower H_2O absorption line strengths for this band), and (3) maximize the signal-to-noise ratio of the multi-alkali photomultiplier tube (PMT) used in the receiver. The larger sky radiance background is a disadvantage of this choice. The gain curve of alexandrite lasers ranges from approximately 725 to 790 nm, facilitating the use of a pulsed alexandrite transmitter operating at the moderate-line strength (2.0×10^{-23} cm^2 molecule^{-1} cm^{-1}) 729.23-nm vacuum wavelength H_2O vapor transition.[12] Although more suitable lines exist in the 718–727-nm range, the practical difficulties associated with operating a broadband laser at the edge of the gain curve wing prohibited their use.

The HAL transmitter (Fig. 1) utilizes a master–slave configuration in which a flashlamp-pumped, pulsed alexandrite ring laser (Light Age Pro-PAL 101) serves as the slave cavity and is injection seeded by a continuous-wave, narrow-bandwidth extended cavity diode laser (ECDL) designed by Toptica (DL100), which serves as the master laser. The seed beam is coupled into the pulsed laser cavity by a polarization-preserving, single-mode fiber and interferes with itself on successive trips through the slave cavity. A photodiode located inside the alexandrite cavity is used to trigger the Q-switch when the interference signal amplitude exceeds a user-set threshold voltage. Large interference spikes occur when the

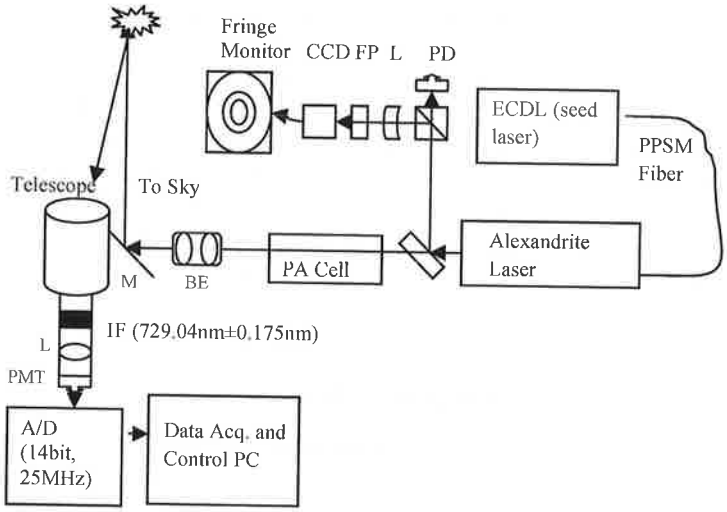

Fig. 1. LIDAR optical train: ECDL, extended cavity diode laser; PPSM fiber, polarization-preserving single-mode fiber; PA, H_2O photo-acoustic absorption cell; PD, fast photodiode; L, lens; FP, Fabry–Perot etalon; M, mirror; BE, beam expander; IF, narrowband interference filter; and PMT, photomultiplier tube.

seed beam comes into resonance with one of the alexandrite laser cavity modes, with the largest spike occurring closest to the time of peak alexandrite laser gain. The threshold is set such that this spike triggers the Q-switch, as opposed to one of the smaller spikes that occur earlier in the pump pulse. The laser electronic feedback loop adjusts the alexandrite laser cavity length on a pulse-by-pulse basis (via a piezocrystal mounted to one of the cavity mirrors) to keep the largest spike centered in a 40-μs window near the time of peak gain, resulting in a 100-ns, single-mode laser pulse centered at the seed laser frequency. The 100-ns pulse width limits the LIDAR range resolution to 15 m. Single-mode operation of the alexandrite laser assures (for cavity longitudinal mode spacing of approximately 160 MHz) that the transmitter bandwidth satisfies our above-stated criteria of narrow linewidth. The two operating wavelengths are alternately derived by applying an appropriate sine voltage waveform (Sec. 2.3) to a piezo-crystal mounted on the ECDL diffraction grating. Operating parameters of both lasers are given in Table 1.

A small fraction of the pulsed laser output energy is used to trigger the data acquisition electronics and to illuminate a high-finesse 10-GHz etalon for real-time qualitative

Table 1. Laser parameters for Toptica DL100 seed laser and Light Age Pro-PAL 101 pulsed laser

Diode seed laser	Pulsed alexandrite laser
Power = 5 mW (after fiber)	Pulse energy = 45 mJ
Linewidth ~1 MHz	Linewidth < 160 MHz
Course tuning range = 725–734 nm	Rep. rate = 25 Hz
Fine tuning range = 30 GHz	Pulse width = 100 ns
Mode = TEM_{00}	Divergence = 500 μrad (after beam expander)
	Pulse-to-pulse energy fluctuations = ±10%

monitoring of laser spectral purity. The main beam passes through a photo-acoustic (PA) H_2O cell,[6] which serves as a laser frequency monitor. A pressure wave (whose amplitude is proportional to H_2O absorption and laser power) is created within the cell when the laser beam is resonantly absorbed by water vapor molecules. The detected wave is filtered and amplified using a low-noise preamplifier (Stanford Research Systems SRS 560) and digitized. The digitized signal is used to sort the on- and off-resonance pulses and to deduce laser frequency, via comparison with a calibration scan of the 729.23-nm H_2O vapor line. After traversing the cell, the main beam is expanded to 25 mm to reduce the divergence to less than 500 μrad and is then directed by two beam-steering mirrors into the atmosphere along an axis parallel to the receiver telescope.

2.2. Receiver

Backscattered light for each laser pulse is collected by a 30-cm Cassegrain telescope with an adjustable iris located at the telescope focus. The iris is adjusted until the receiver field of view slightly exceeds the ($\sim$500 μrad) laser divergence angle in order to minimize sky background signal during daytime operation. The transmitter and receiver axes are parallel and separated by 30 cm (bistatic LIDAR configuration) for the initial studies in order to minimize intense backscattering from low altitudes, which otherwise would result in damage to the PMT. Backscattered light exiting the telescope is recollimated and then passes through a narrowband (FWHM = 0.35 nm) Barr interference filter, which transmits 70% of laser backscatter while attenuating nearly all of the broadband background light. The filtered light is then imaged onto a side-on, multi-alkali cathode PMT (Hamamatsu R3896). To reduce saturation effects during daytime hours, the PMT is gated during all times except 3–200 μs after laser pulse emission (corresponding to the range 450 m–30 km). A 14-bit, 25-MHz analog-to-digital (A/D) converter (Gage Octopus 8322) is employed to amplify and digitize the backscatter signal from the PMT. One observed drawback of the employed gating method is distortion in the first 1 km of LIDAR backscatter return. PMT nonlinear effects and incomplete overlap between telescope and transmitter fields of view at low altitudes limit the lower end of the prototype LIDAR range to 1.5 km at night and 1.8 km during daytime. This problem will be addressed in a modified receiver design.

2.3. DIAL control and data acquisition

HAL control and data acquisition hardware are shown in Fig. 2. A calibration scan of the PA absorption spectrum at the 729.23-nm H_2O vapor line was performed [Fig. 3(a)] before data acquisition commenced in order to determine the diode seed laser control voltages corresponding to the LIDAR operating wavelengths λ_{ON} and λ_{OFF} . The measured absorption spectrum was first fitted to a Lorentzian function to smooth small-scale noise. During data acquisition, a 12.5-Hz sine wave is generated by software, written to a digital-to-analog converter (D/A), and applied to the seed laser diffraction grating controller to vary the seed frequency. The wave amplitude, offset, and phase are adjusted so that the sine wave peak voltage coincides with λ_{ON} and the trough voltage corresponds to λ_{OFF}, which in the preliminary studies was located approximately 9 GHz [see Fig. 3(a)] from the absorption peak. A synchronized digital waveform is also generated via software to trigger the alexandrite laser flashlamp pulse near each sine wave peak and trough, thereby producing 25-Hz laser pulses, which alternate between the two operating wavelengths. A fast photodiode detects each transmitter pulse leaving the laboratory and triggers both the

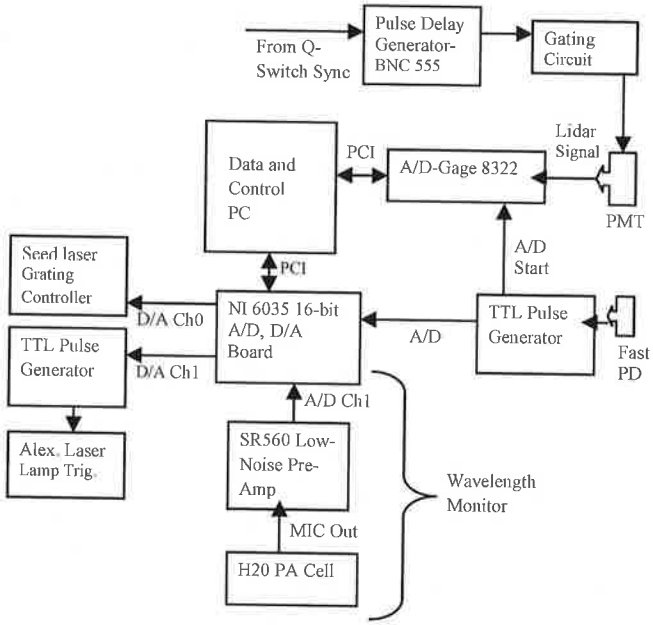

Fig. 2. LIDAR acquisition and control electronics. A small fraction of the outgoing laser pulse illuminates the fast photodiode (PD) to trigger acquisition electronics. The majority of light passes through the photo-acoustic (PA) cell, which is used for wavelength monitoring. The backscattered laser radiation is detected by the PMT (photomultiplier tube). A/D, analog-to-digital converter; D/A, digital-to-analog converter.

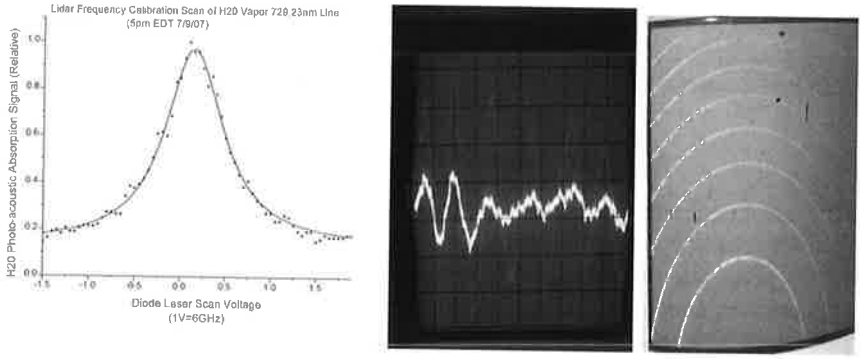

(a) (b) (c)

Fig. 3. LIDAR transmitter frequency characterization. (a) LIDAR calibration scan of H_2O vapor PA signal. The data points are fitted to a Lorentzian function. (b) H_2O PA absorption signal when cell is illuminated by pulsed LIDAR beams centered at at λ_{ON} (larger signal appearing as faint trace) and at λ_{OFF} (smaller signal appearing as brighter trace). (c) Transmission of pulsed LIDAR beam through a 10-GHz Fabry–Perot etalon, indicating single longitudinal operation of pulsed slave cavity.

Gage 14-bit, high-speed A/D converter used to digitize the backscattered at 25 megasamples per second (MS/s) and the National Instruments (NI 6035E) 16-bit A/D used to digitize the H_2O PA signal. The PA waveform [Fig. 3(b)] is analyzed in real time to properly sort the LIDAR waveforms according to wavelength. Such sorting is necessary to prevent a missed trigger (from a fast photodiode) from mixing the returns at λ_{ON} and λ_{OFF}. Quality assurance tests were built into the software to discard backscattered LIDAR waveforms contaminated by after pulsing of the alexandrite laser or PMT, which, by completely different mechanisms, produce secondary PMT pulses approximately 5–20 μs after the primary laser pulse and thereby distort the detected signal. The LIDAR and PA waveforms at each operating wavelength are averaged over 30–60-s intervals to improve the signal-to-noise ratio and archived to disk. The software also utilizes the H_2O PA waveforms to determine the H_2O differential absorption cross section (used by the data analysis algorithm to calculate H_2O density) and to further reject any profiles that may be corrupted by poor laser spectral purity. Fabry–Perot fringes [Fig. 3(c)] from the diagnostic etalon [imaged onto a charge-coupled device (CCD)] provide a real-time qualitative indication of single-mode transmitter operation. Preliminary testing revealed that the automated LIDAR is capable of continuous operation over periods exceeding 30 h under reasonably stable laboratory thermal conditions but also that the transmitter performance is very sensitive to changes of more than $\pm 3^{\circ}$C at laboratory temperatures.

3. HAL Data Analysis

The DIAL equation[9] is used to invert detected LIDAR backscatter profiles, yielding H_2O vapor density profiles:

$$n_{H_2O}(z) = \frac{1}{2 \cdot \Delta\sigma_{H_2O}} \frac{d}{dz} \ln\left(\frac{P_{OFF}(z)}{P_{ON}(z)}\right) + \Delta n_{\beta}(z) + \Delta n_{e}(z). \tag{1}$$

In Eq. (1), $n_{H_2O}(z)$ is the water vapor number density (molecules/cm^3) at altitude z (cm), $\Delta\sigma_{H_2O} = \sigma_{ON} - \sigma_{OFF}$ is the H_2O differential absorption cross section (cm^2) between the LIDAR operating wavelengths λ_{ON} and λ_{OFF}, and $P(z)$ represents the detected light backscattered from range z at either the on- or off-resonance wavelength. The terms $\Delta n_{\beta}(z)$ and $\Delta n_{e}(z)$ represent the backscatter and extinction correction terms. Accurate estimates of these terms are often not possible (especially in turbid media), and they are often neglected (to first order) for LIDARs with small-wavelength separations (on the order of a few gigahertz, as in this case) that switch back and forth between the operating wavelengths on the timescale of milliseconds. In addition, we have neglected the temperature dependence of $\Delta\sigma_{H_2O}$ (mainly through σ_{ON}) for the prototype LIDAR study, which can produce errors in the H_2O vapor profiles[3] due to unknown temperature distribution along the line of sight. To minimize the resulting error in H_2O number density retrievals, we have selected an H_2O absorption line with a lower state energy of 325 cm^{-1}, which is close to the optimal range (70–300 cm^{-1}) suggested by Browell for temperature insensitivity of H_2O number density retrievals and which lies in the suggested optimal range (220–550 cm^{-1}) for H_2O mixing ratio retrieval temperature insensitivity. Lines with lower state energies in the range that we used are also more temperature sensitive (according to Browell's criterion) for temperatures below 250 K, which was not the case during our initial summer measurements at altitudes <5 km.

HAL backscattered signal profiles $P(z)$ at the on- and off-resonance frequencies (Fig. 4) are first averaged over the desired integration time (often 30 s for LIDAR backscatter

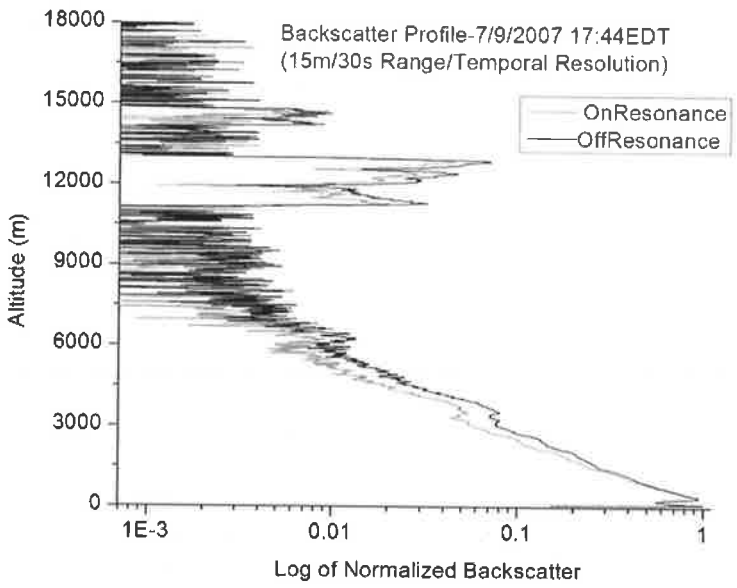

Fig. 4. Sample relative LIDAR backscatter profiles (arbitrary units) at the on-resonance (gray trace) and off-resonance (black) HAL operating frequencies. The small dip in the low-altitude backscatter profiles (first few hundred meters) is the result of PMT gating. The backscattered intensity is normalized to the maximum backscattered intensity.

profiles and 6 min for H_2O vapor profiles), and the average background is subtracted. The profile of $\ln(P_{OFF}/P_{ON})$ is formed, and the numerical derivative of the result is computed for each altitude z by applying a linear-regression fit to a user-specified number of points centered at each altitude z (defining the range resolution). The slope of this line is assigned to the value of derivative at altitude z. Owing to lower signal-to-noise ratios at higher altitudes, the number of points used in the fit increases linearly with altitude. The differential absorption cross-section $\Delta\sigma_{H_2O}$ is calculated using the PA waveforms for both operating wavelengths and the calibration scan [Fig. 3(a)]. Water vapor profiles currently extend from approximately at 1.5 to 5 km at night and 1.5 to 4 km during daytime hours.

4. Initial LIDAR Tests and Discussion

HAL transmitter capabilities and limitations were thoroughly evaluated during July 2006 field testing. The prototype LIDAR was pointed vertically to obtain profiles of absolute humidity and LIDAR backscatter. Nighttime water vapor measurement performance was evaluated via simultaneous colocated radiosonde launches on July 18 and 19. The LIDAR was modified in June 2007 to incorporate daytime measurement capability and was further automated to improve and simplify the data control and acquisition process (see Sec. 2.3). The modified system was then tested to determine its capability for short-term front and cloud prediction. Although regional radiosonde launches provided the only comparison of daytime measurements, a colocated microwave radiometer was available on the night of August 12, 2007, for 7 h of H_2O vapor comparisons as a cold front moved into the area. Each of the comparisons is discussed in this section.

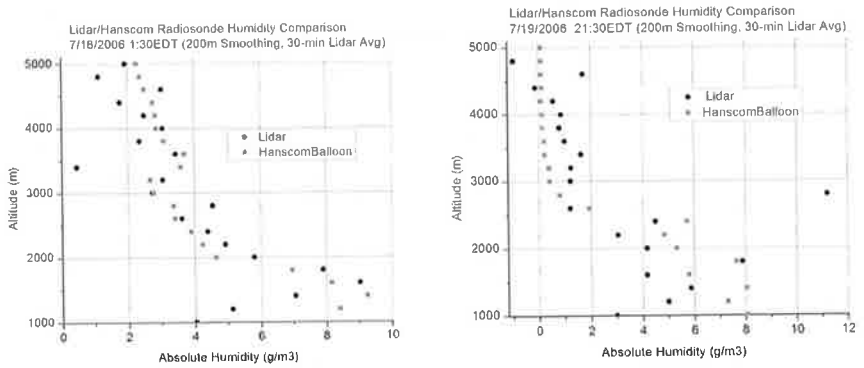

(a) (b)

Fig. 5. Absolute humidity profiles obtained by HAL and Vasaila-92 radiosonde. The profiles are plotted as points at comeasured altitudes for ease of comparison, and LIDAR profiles are averaged over 30 min to account for the finite balloon transit time. Absolute humidity values less than zero are obviously unrealistic but are included for comparison.

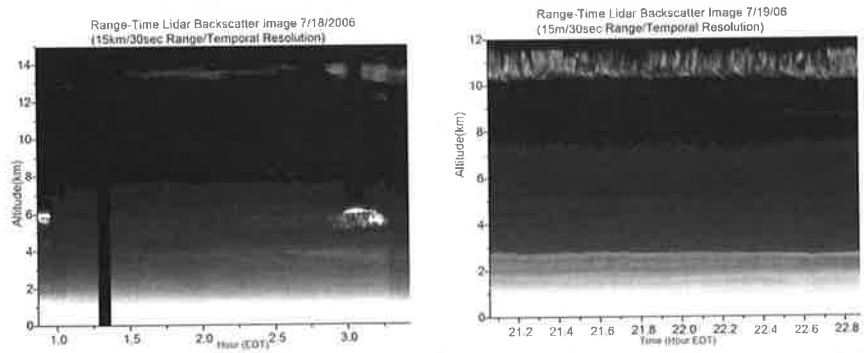

(a) (b)

Fig. 6. Relative LIDAR backscatter range–time plots for portions of July 18 and 19. Grayscale levels are proportional to relative LIDAR backscatter (arbitrary units), with white (black) denoting areas of space/time with maximum (minimum) backscatter. The black vertical line in the left-hand figure is due to missing data during a short period of laser reoptimization.

The Vaisala RS92-SGP radiosonde used in the July 2006 comparisons contains highly accurate pressure, temperature, and relative humidity (RH) sensors, although capacitive hygrometer RH measurements under conditions of very low and high humidities are prone to larger errors. Comparisons between radiosonde- and LIDAR-derived absolute humidity profiles are shown in Fig. 5, and the LIDAR relative backscatter images for both nights (during the periods near launch) are shown in Fig. 6. The radiosondes were launched less than 100 m from the LIDAR and provide the most direct comparison with LIDAR-derived H_2O vapor profiles, although complete agreement is not to be expected, due to wind-induced balloon drift during the ascent. To facilitate direct comparison, radiosonde-derived H_2O vapor mixing ratios are combined with radiosonde-measured temperature and

pressure to calculate absolute humidity. LIDAR-derived H_2O molecular density profiles [via Eq. (1)] are converted to absolute humidity via knowledge of the H_2O vapor molar mass (18.01 g/mole). The LIDAR- and radiosonde-derived H_2O absolute humidity profiles agreed to better than $\sim$1 g/m^3 on July 18 and 2 g/m^3 on July 19 for altitudes of 1.5 km to near 5 km, with the exception of anomalies near 3.4 km on July 18 and near 2.8 km on July 19. The anomalies are most likely associated with significant backscatter gradients near these altitudes, as can be seen in Fig. 6. The LIDAR data inversion method is often prone to large errors near these regions unless sophisticated data analysis methods are employed and auxiliary measurements near these altitudes are available. The above-stated agreement lies within the accuracy range required for tactical laser applications (see the Introduction). Disagreement below 1.5 km is most likely due to LIDAR PMT saturation. Another possible contribution could be incomplete overlap between the LIDAR transmitter beam and the telescope field of view at low altitudes, although this effect is in principle canceled by the ratio method employed in the H_2O DIAL inversion algorithm [Eq. (1)] and is in practice satisfied if both laser frequencies are derived from the same seed beam (so that both transmitter beams have the same overlap functions).

Vertical profiles of detected LIDAR-relative backscatter at the off-resonance frequency can be used to produce range–time plots, such as those shown in Fig. 6. The grayscale levels are proportional to the backscattered intensity at the given time from a given altitude. It should be noted that the total received LIDAR backscatter includes Mie scattering contributions from aerosols and Rayleigh scattering from clean-air molecules. For the prototype LIDAR, no attempt was made to subtract the better-known Rayleigh scattering (long-term climatological mean vertical profiles of pressure and temperature will be used for operational LIDAR when colocated temperature and pressure profiles are not available) or to correct the backscattering for aerosol extinction. Nevertheless, qualitative information regarding aerosol layers and cloud locations can be inferred. As can be seen from Figs. 4 and 6, the HAL system is capable of high-resolution backscatter retrievals up to nearly 15 km. Such plots are often used to assess convective features and other dynamical phenomena, in addition to determining cloud base heights, and to detect the presence of aerosol layers (via large gradients in relative backscattering). The July 19 profile, for instance, reveals negligible backscattering above 3 km, except for a persistent cirrus cloud layer near 11 km that occurred near a region of high wind shear and turbulence. The atmosphere was very dry on this evening, based on surface observations and radiosonde profiles. This is in contradiction to July 18, which was much warmer and more humid. On July 18, backscatter is observed up to 6 km, in addition to scattering from a thin high cirrus layer near 14 km.

Daytime H_2O vapor measurements pose the largest technical challenge for any water vapor/aerosol LIDAR, due to the difficulty of detecting small signal differences (between the operating wavelengths) in the presence of large sky background radiance. Representative H_2O water vapor profiles acquired during summer daytime hours are shown in Figs. 7(a) and 7(b). July 3, 2007, was a dry, fair-weather day in the northeast United States, with clear skies giving way to fair-weather cumulus clouds above Hanscom Air Force Base around 11 a.m. EDT. Intense backscattering from the low-altitude clouds ($\sim$1.5–2 km) forced suspension of LIDAR data taking. Figure 7(b) contains comparisons of HAL early morning profiles with radiosonde launches (8 a.m. EDT) from Albany, New York; Chatham, Massachusetts; and Grey, Maine. These sites range from 130 to 300 km away from Hanscom Air Force Base, so the comparisons must be kept in perspective. One common feature of all summer daytime profiles (based on similar comparisons) was the underestimation of H_2O vapor below 1.8 km (as compared to $\sim$1.5 km during nighttime hours). Further testing revealed that PMT

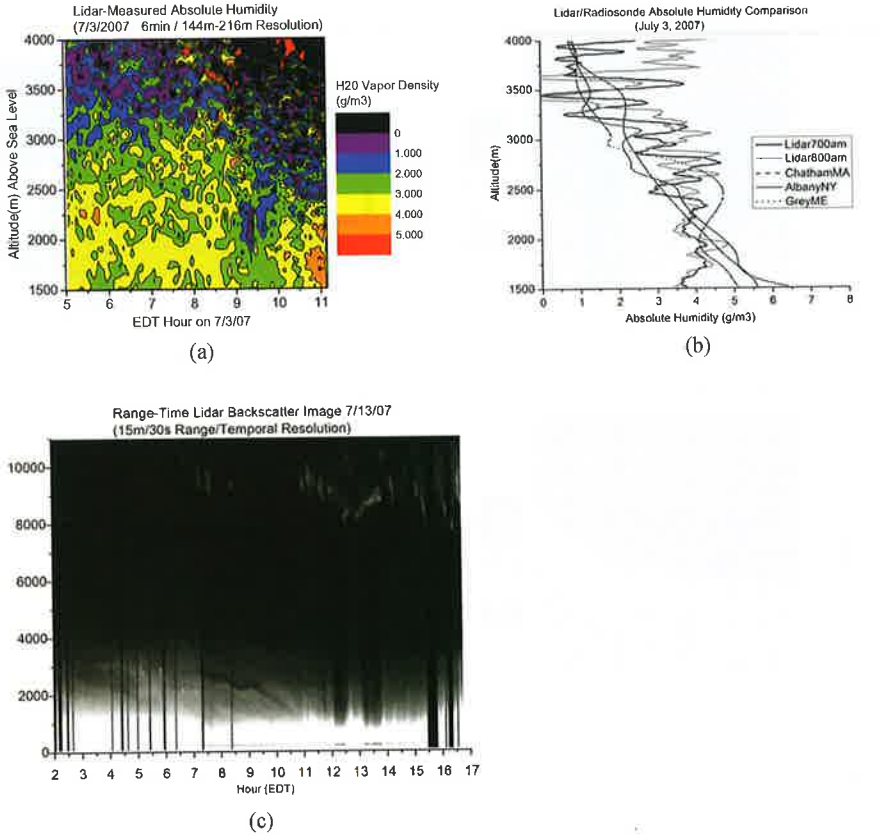

Fig. 7. Daytime LIDAR measurements of H_2O vapor and relative LIDAR backscatter range–time plot. Comparisons of absolute humidity with radiosonde launches from Chatham, Massachusetts; Grey, Maine; and Albany, New York, are provided for qualitative estimation of daytime HAL performance.

saturation from the combination of sky radiance transmitted by the interference filter and the strong low-altitude scattering is the likely cause of this. In addition, the daytime upward-pointing vertical range limit for H_2O vapor (imposed by a lower signal-to-noise ratio during daylight) is approximately 3.5 km during morning hours, decreasing to slightly below 3 km near local noon. The downward-pointing operational LIDAR will not experience such large background radiances. A dual-interference filter receiver design that eventually will incorporate a combination of modified analog detection at low altitudes and photon counting above ~3 km should increase the measurement range during both night and daytime hours. Figure 7(c) shows 15 consecutive hours of LIDAR relative backscatter measurements taken on July 13, 2007. Water vapor measurements on this very warm day were poor, due to laser frequency instability caused by laboratory air-conditioner malfunctioning. Despite laser instability, the evolution of cloud and boundary layer heights (characterized by very sharp gradients in backscattering) and aerosol layers are easily detected during all hours.

One potentially useful application of HAL involves using humidity measurements to predict clouds and incoming fronts. A modified version of the Radiometrics WVP-1500

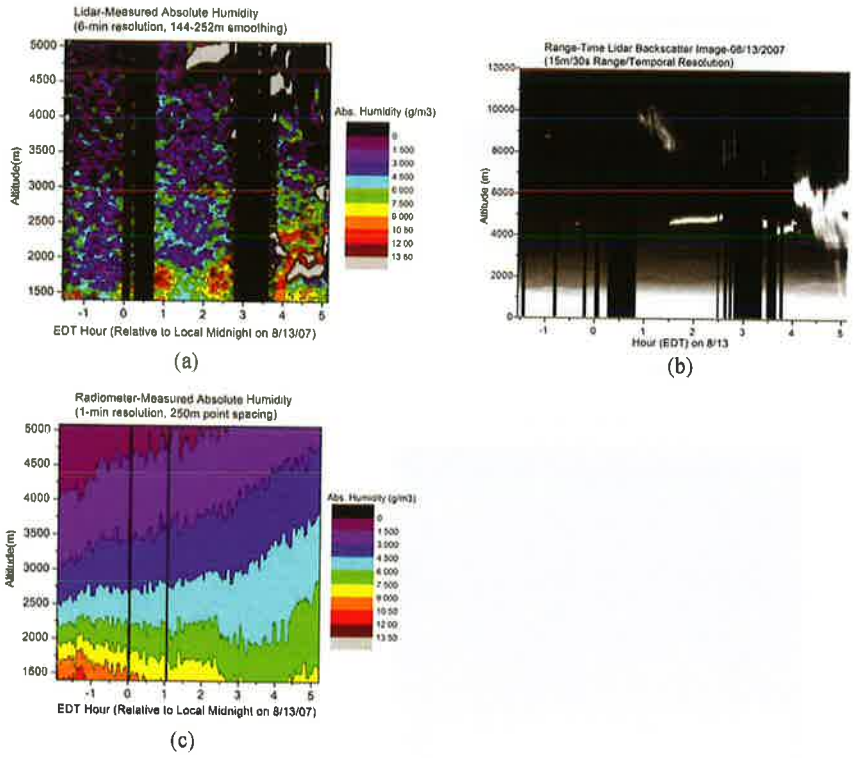

Fig. 8. LIDAR-microwave radiometer absolute humidity comparison and relative LIDAR backscatter range–time plot.

water vapor–profiling microwave radiometer was employed along with HAL on the night of August 12, 2007, in advance of an approaching front. LIDAR- and radiometer-derived absolute humidity and relative LIDAR backscatter images are shown in Fig. 8.

The Radiometrics microwave radiometer derives water vapor profiles by applying an artificial neural networking algorithm to path-integrated irradiances (at a programmed sequence of radiometer antenna tipping angles) measured at a number of frequencies between 22 and 30 GHz, produced by the pressure-broadened atmospheric H_2O vapor emission line centered at 22.2 GHz. Although radiometer profiles are output at 250-m altitude bins from 1 to 10 km, the vertical resolution of similar passive water vapor profilers (limited by the weighting function) has been estimated[8] to be 0.7–1 km for altitudes between 1 and 4 km. As such, comparisons between LIDAR- and radiometer-derived water vapor profiles must be placed in the proper context. With the exception of LIDAR-derived H_2O vapor underestimation below 1.5 km (due to PMT saturation effects), the profiles are in reasonable agreement when differences in resolution (and the accompanying noise) are taken into account. Both measure comparable amounts of water vapor and indicate increases in H_2O vapor above 2 km as the front approached (after 4 a.m. EDT). One noticeable difference is that the radiometer profiles show a drying trend at altitudes below 2,000 m until 4 a.m., whereas the LIDAR profiles indicate a moistening trend during these hours. Further analysis of LIDAR data at coarser resolution reaffirmed this trend, dismissing resolution difference as a possible reason for the discrepancy. Local surface

dewpoint observations taken at this time were consistent with radiometer-derived absolute humidity values near 2 km and were not consistent with LIDAR-derived values. Cloud layer thickening with time was observed [see Fig. 8 (b)], and the multiple-scattering effect from cloud layers would be more likely to contaminate the LIDAR H_2O vapor profiles (below the clouds at ~2–3 km) than the radiometer profiles, whose employed frequencies are much less sensitive to cloud effects. Local surface observations still reported clear skies until 6 a.m., although the reports based on the laser ceilometers typically employed provide cloud information only up to 4 km. Further measurements taken under similar meteorological conditions will be necessary to determine whether the LIDAR possesses capability to sense incoming clouds via increased absolute humidity measurements just before cloud formation.

5. Conclusions

The capabilities and limitations of the prototype version of HAL have been thoroughly evaluated in this initial study. The transmitter produces high-energy, narrow-bandwidth pulses at precisely characterized frequencies for more than 30 h of unattended operation (under stable thermal conditions). Comparisons with colocated radiosondes revealed good qualitative and quantitative agreement (according to accuracy requirements outlined in the Introduction) in the upward-pointing nighttime absolute humidity profiles from 1.5 km to nearly 5 km. Qualitative comparison with regional radiosondes during daytime hours were used to test the upward-pointing range, which is limited by intense sky radiance to 3.5 km or less. These effects will be smaller for the operational downward-pointing LIDAR, whose aperture (and hence range) is also scalable by a factor of two. Comparisons with a colocated microwave radiometer yield qualitative absolute humidity agreement for altitudes ~2–4.5 km and possible cloud contamination of LIDAR-derived profiles below 2 km. More tests are needed before any conclusive statements regarding the LIDAR's ability to sense incoming clouds (via humidity profiles) can be made. One limitation of the bistatic upward-pointing prototype design is the inability to accurately measure water vapor below 1.5 km during nighttime hours and below ~8 km during daytime hours. An improved receiver design, when implemented, should reduce the lower range limit to less than 1 km while also increasing the upper range limit. HAL is also capable of retrieving high-resolution relative backscattering from aerosol layers and clouds up to 10–15 km under both day and night conditions, from which boundary layer and cloud evolution and heights can be inferred via steep gradients in LIDAR backscattering.

6. Acknowledgments

The authors would like to thank AFRL scientists John Roadcap and Donald Norquist for helpful meteorology discussions, Pat McNicholl for providing useful technical advice, and Anthony Dentamaro for his willingness to help whenever needed. AFRL personnel George Clement and Paul Desrochers provided support for the radiosonde and microwave radiometer instruments, respectively. Finally, we wish to thank Robert Beland and Major Brian Griffith for their support for the project. The research was conducted at the Air Force Research Laboratory, Hanscom Air Force Base (Bedford, Massachusetts), with the support of the High Energy Laser Joint Technology Office program for the initial construction of HAL.

References

[1]Ackermann, J., J. Atmos. Oceanic Technol. **15**, 1043 (1998).

[2]Armstrong, R.L., Appl. Opt. **23**, 148 (1984).

[3]Browell, E.V., S. Ismail, and B.E. Grossmann, Appl. Opt. **12**, 1517 (1991).

[4]Browell, E.V., T.D. Wilkerson, and T.J. McIlrath, Appl. Opt. **18**, 3474 (1979).

[5]Dao, P.D., and A.E. Dentamaro, "Development of a Deployable Aerosol/Water Vapor Lidar to Characterize the Atmosphere," *SPIE AeroSense 2003*, Orlando, FL (April 2003)

[6]Dentamaro A.E., and P.D. Dao, Rev. Sci. Instrum. **74**(7), 3502 (2003).

[7]Friehe, C.A., J.C. La Rue, F.H. Champagne, C.H. Gibson, and G.F. Dreyer, J. Opt. Soc. Am. **65**(12), 1502 (1975).

[8]Guldner, J., and D. Spankuch, J. Atmos. Oceanic Technol. **18**, 925 (2000).

[9]Kovelov, V., and B. Eichinger, *Elastic Lidar—Theory, Methods, and Analysis*, Wiley, New York (2004).

[10]Norquist, D., Air Force Geophysical Research Laboratories, Hanscom Air Force Base, private communications (2007).

[11]Norquist, D.C., P.R. Desrochers, P.J. McNicholl, and J.R. Roadcap, J. Appl. Meteorol. Climatol. **47**, 1322 (2008).

[12]Rothman, L.S., D. Jacquemart, A. Barbe, D.C. Benner, M. Birk, L.R. Brown, M.R. Carleer, C. Chackerian, Jr., K. Chance, L.H. Coudert, V. Dana, V.M. Devi, J.M. Flaud, R.R. Gamache, A. Goldman, J.M. Hartmann, K.W. Jucks, A.J. Maki, J.Y. Mandin, S.T. Massie, J. Orphal, A. Perrin, C.R. Rinsland, M.A.W. Smith, J. Tennyson, R.N. Tolchenov, R.A. Toth, J. Vander Auwera, P. Varanasi, and G. Wagner, J. Quant. Spectrosc. Radiat. Transfer **96**, 139 (2005).

[13]Schotland, R.M., "Some Observations of the Vertical Profile of Water Vapor by Means of a Ground-Based Optical Radar," *Proceedings of the Fourth Symposium on Remote Sensing of Environment* (October 1966).

[14]She, C.Y., Contemp. Phys. **31**(4), 247 (1990)

[15]Westerman, S.D., and N. C. Mehta, Proc. SPIE **1221**, 294 (1990).

[16]Wulfmeyer, V., and C. Walther, Appl. Opt. **40**(30), 5304 (2001).

The Authors

Dr. Phan Dao is currently the principal investigator of the Space Object Surveillance Technologies program at the Air Force Research Laboratory, Space Vehicles Directorate, Hanscom Air Force Base. He develops space-based sensor techniques. Prior to his activities in space technology, he developed and applied LIDAR techniques for atmospheric diagnostics. His first job was with the Chemical Laser group at KMS Fusion, Ann Arbor, Michigan. He received a Ph.D. in physics from the University of Colorado in Boulder in 1985.

Dr. James Sherman is an associate professor of physics and astronomy at Appalachian State University. He is also cofounder and research scientist at the newly created Appalachian Atmospheric Interdisciplinary Research research facility, which has formed collaborations with atmospheric research groups at NOAA, NASA, and other universities to study the effects of aerosols on regional climate, air quality, and vegetation. He received his Ph.D. in physics from Colorado State University, where he worked on sodium resonance Doppler LIDAR development for mesopause region thermal/dynamical studies. He received the M.S. in optical engineering from the University of Rochester and the B.S. in physics from Iowa State University.